LETTERS

Evidence for an ancient martian ocean in the topography of deformed shorelines

J. Taylor Perron[1]†, Jerry X. Mitrovica[2], Michael Manga[1], Isamu Matsuyama[3] & Mark A. Richards[1]

A suite of observations suggests that the northern plains of Mars, which cover nearly one third of the planet's surface, may once have contained an ocean[1–7]. Perhaps the most provocative evidence for an ancient ocean is a set of surface features that ring the plains for thousands of kilometres and that have been interpreted as a series of palaeoshorelines of different age[1,7]. It has been shown, however, that topographic profiles along the putative shorelines contain long-wavelength trends with amplitudes of up to several kilometres[4,5,8], and these trends have been taken as an argument against the martian shoreline (and ocean) hypothesis[8]. Here we show that the long-wavelength topography of the shorelines is consistent with deformation caused by true polar wander—a change in the orientation of a planet with respect to its rotation pole—and that the inferred pole path has the geometry expected for a true polar wander event that postdates the formation of the massive Tharsis volcanic rise.

Parker *et al.*[1,3] and Clifford and Parker[7] used an array of geologic and topographic features to identify several possible palaeoshorelines near the margins of the northern plains of Mars. Two of these can be traced without major interruptions for thousands of kilometres (Fig. 1): the Arabia shoreline (contact 1 of refs 1 and 3), which coincides roughly with the dichotomy in crustal thickness between the northern and southern hemisphere, and the Deuteronilus shoreline (contact 2 of refs 1 and 3), which is inferred to be younger because it is encircled by the Arabia shoreline and is less degraded. However, subsequent studies have challenged the notion that these features are shorelines[9]. The most basic objection stems from the observation that topographic profiles along the contacts do not follow surfaces of equal gravitational potential (that is, sea level)[4,5,8], as the margins of a standing body of water should. In particular, the contacts contain significant long-wavelength trends, with amplitudes of ~2.5 km for Arabia and ~0.7 km for Deuteronilus (Fig. 1).

The antiquity of the putative shorelines (at least 2 billion years (Gyr), the age of most of the northern plains surface[10]) allows for the possibility that they have been subject to long-wavelength, large-amplitude deformation since their formation. On Earth, true polar wander—TPW, the reorientation of the planet relative to its rotation pole—has been implicated in very-long-wavelength sea-level variations with timescales exceeding 10^6–10^8 years (refs 11, 12). In the following, we investigate whether TPW also provides a plausible explanation for the observed deformation of the Arabia and Deuteronilus contacts on Mars. That is, we seek a TPW path that is consistent with the displacements of these contacts away from an ancient equipotential surface, and that is compatible with the basic physical principles governing the rotational dynamics of a terrestrial planet.

The present-day figure of Mars provides an important constraint on the expected geometry of any TPW event that postdates the

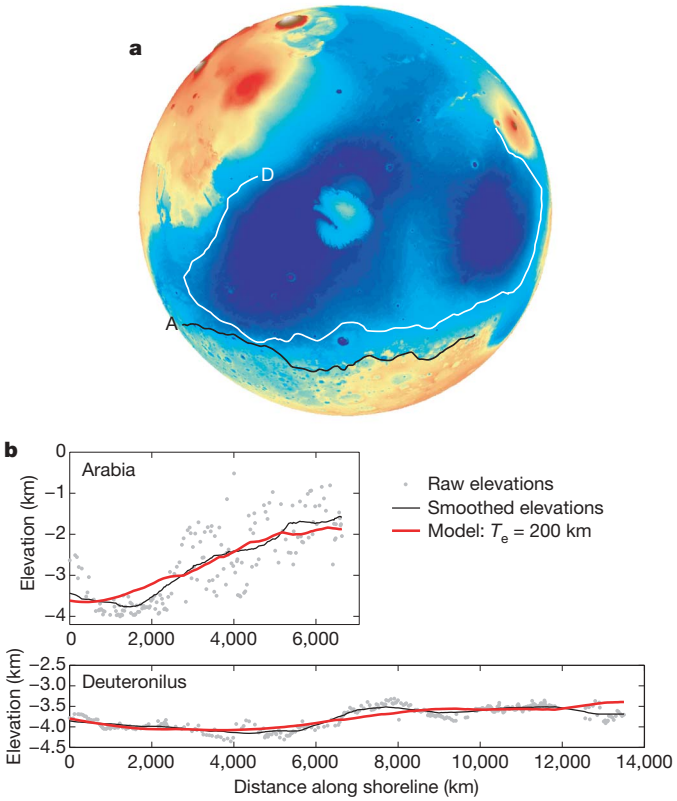

Figure 1 | Possible palaeoshorelines on Mars. a, Map of the northern hemisphere of Mars showing the portions of the hypothesized Arabia (black line A) and Deuteronilus (white line D) shorelines used in our analysis. Shoreline locations are from Carr and Head[8]. Orthographic spherical projection centred on the north pole. To avoid joining contacts that may have been formed at different times or by different processes, we used the longest section of each shoreline that can be traced continuously. This also avoids portions of the shorelines that may have been modified by more recent processes, such as erosion and sedimentation near the outflow channels in Chryse Planitia, crustal intrusion near Olympus Mons and west Tempe Terra, and sedimentary infilling in Isidis. **b**, Topographic profiles along the Arabia and Deuteronilus shorelines, beginning at locations A and D. The points are Mars Orbiter Laser Altimeter (MOLA) elevations reported by Carr and Head[8], and the black lines are 2,000 km moving averages. The short-wavelength scatter arises at least in part from generalization of the mapped shorelines in areas of complex topography[8], and detailed examination of these regions[30] suggests that the actual short-wavelength variations in elevation are small. Vertical and horizontal scales are the same for both profiles. Elevations are relative to the present-day 6 mbar geoid. Red lines are fits of equation (3) to the unsmoothed shoreline elevations for T_e = 200 km (see Methods and Table 1).

[1]Department of Earth & Planetary Science, University of California, Berkeley, California 94720, USA. [2]Department of Physics, University of Toronto, Ontario M5S 1A7, Canada. [3]Department of Terrestrial Magnetism, Carnegie Institution of Washington, Washington DC 20015, USA. †Present address: Department of Earth and Planetary Sciences, Harvard University, Cambridge, Massachusetts 02138, USA.

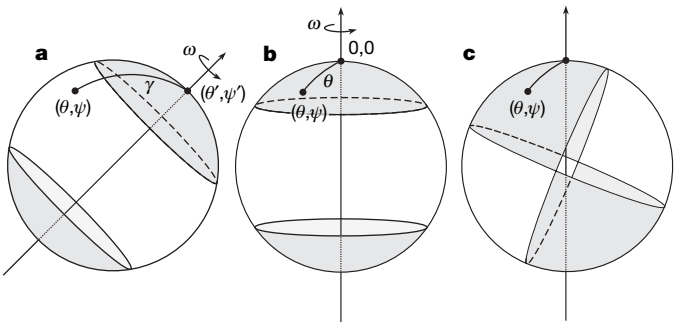

Figure 2 | Changes in topography due to TPW. a and **b** show the geographically variable component of the centrifugal potential for a TPW event that displaces the north pole of a planet with rotation rate ω from some original position (θ', ψ') (**a**) to the present orientation (**b**). In each state, the centrifugal potential is defined by a degree-two, order-zero spherical harmonic (that is, an oblateness term) plus a constant term, as illustrated by the shading. The change in the potential, and the associated change in topography, is characterized by a degree-two, order-one 'quadrential' geometry (**c**). These changes are zero along two great circles perpendicular to the pole path. The first great circle includes the point halfway along the (great circle) arc joining the initial and present pole position, and the second great circle is perpendicular to the first. The perturbation reaches a maximum value at four sites along the great circle that includes the pole path, 45° from the zeroes. The amplitude of the perturbation in the potential is a function of the displacement of the pole, while the topographic deflection associated with this perturbation is also a function of the thickness of the elastic lithosphere T_e (see Methods). The point (θ, ψ) represents an observation site fixed to the surface geography. All geographic coordinates are relative to the final pole location.

formation of the Arabia and Deuteronilus contacts. The long-term motion of a planet's rotation axis is controlled by the orientation of the non-hydrostatic geoid at spherical harmonic degree two[13,14]. On Mars, the degree-two, non-hydrostatic geoid is dominated by the Tharsis rise[15], an immense volcanic construct centred slightly north of the equator[16]. The emplacement of an excess mass such as Tharsis will drive TPW that brings it to a position closer to the equator[13], although this tendency may be inhibited by the presence of an elastic lithosphere[14,17] (see Supplementary Information). Equivalently, an excess mass near the equator will also resist a reorientation that would move it further from this position. Thus, any TPW of Mars occurring after the emplacement of Tharsis should, if driven by a load smaller than Tharsis, be constrained to follow a path that keeps Tharsis near the equator; such a path would be a great circle 90° from the centre of Tharsis[17].

If a TPW event deformed the Arabia and Deuteronilus contacts, it would probably have been constrained to this geometry, because the contacts appear to be younger than Tharsis. The maps of Parker *et al.*[1] and Clifford and Parker[7] indicate that the Deuteronilus contact, and possibly a section of the Arabia contact, follows the outer margin of the Olympus Mons aureole, one of the youngest features on the Tharsis rise. The observation that the outflow channels in Chryse and Amazonis Planitiae, carved by floods that are the most likely source of ocean water[2,5,6], have eroded the outer margins of Tharsis further supports this ordering of ages.

With this physics in mind, we next turn to a direct estimate of palaeopole locations based on the assumption that the contacts are indeed shorelines and that their long-wavelength deformation (Fig. 1) is due to TPW. Polar motion leads to a geographically variable change in a planet's solid surface and geoid (sea surface). On a planet with an elastic lithosphere, these deflections will differ, even after all viscous stresses are relaxed, leading to a non-uniform change in sea level, and therefore also surface topography. The geometry of TPW-induced changes in topography[11,12] is illustrated schematically in Fig. 2. Our search for the palaeopoles followed the procedure described in the Methods. For each shoreline, we identified the palaeopole location that minimizes the misfit between the observed deformation along the contact and the predicted topographic response to the change in centrifugal potential. The topographic response was computed using fluid Love number theory. Table 1 lists the best-fit palaeopoles for various values of the lithospheric thickness T_e and Fig. 3 plots these locations for the specific case $T_e = 200$ km. The fits we obtained (Table 1; thick model line in Fig. 1a for $T_e = 200$ km) demonstrate that deformation associated with TPW can accurately reconcile the observed long-wavelength trends in both shorelines.

These palaeopoles are remarkable for three main reasons. First, the palaeopoles imply roughly 30–60° of net TPW since the formation of the Arabia shoreline and 5–25° since the formation of the Deuteronilus shoreline. These TPW angles are consistent with the relative ages of the shorelines, in the sense that the younger Deuteronilus shoreline corresponds to a pole location closer to the present-day pole. The location of the Arabia palaeopole implies that the oldest ocean was centred in the tropics rather than in the north polar region. Second, the best-fit palaeopoles for both shorelines lie within a few degrees of the same great circle (which passes through the present-day poles along the 335° E meridian), the expected path for TPW driven by an axisymmetric load[13]. This alignment is unlikely to occur by coincidence: the probability of randomly placed points falling this close to the same meridian, and in the appropriate age progression, is less than 0.0025. Nor is the alignment of the palaeopoles likely to be an artefact of background trends in Mars' large-scale topography, given the large difference in amplitude (Fig. 1) between shoreline features that are in close proximity to one another. Finally, the great circle path through the palaeopoles is approximately 90° from the centre of the Tharsis rise (6.7° N, 248.3° E; ref. 16, Fig. 3). As discussed above, this is the expected path of a post-Tharsis TPW event. The probability of randomly placed points falling this close to a great circle 90° from Tharsis is less than 0.0001.

What is the size and orientation of the post-Tharsis load necessary to drive our inferred TPW event? The answer to this question depends on the extent to which Tharsis itself perturbed the rotation pole (see Supplementary Information for a detailed discussion of this point, as summarized below). If the development of Tharsis moved the pole to a location near the great circle path inferred from the shorelines' deformation (Fig. 3), then the equations governing rotational stability suggest that the displacement of the pole was either very small or nearly 90° (refs 14, 17); that is, Tharsis originally formed in either a nearly equatorial or nearly polar location. The former, small Tharsis-driven TPW solution precludes the possibility that surface mass loads were responsible for the post-Tharsis TPW that deformed the shorelines (Fig. 3, Table 1), and in this case internal loads associated with mantle convection were the probable driving mechanism for the TPW. In contrast, if Tharsis drove a large excursion of the pole[18,19], a scenario less favoured in terms of the present-day figure of Mars (see Supplementary Information), then surface loads could have been sufficient to drive the subsequent TPW. In this

Table 1 | Fluid Love numbers and best-fit palaeopole locations

			Arabia			Deuteronilus		
T_e (km)	h_f	$(1 + k_f)$	Latitude, longitude	Z (km)	$\sigma_{r.m.s.}$ (km)	Latitude, longitude	Z (km)	$\sigma_{r.m.s.}$ (km)
100	1.928	2.053	30, 332	−2.55	0.725	66, 340	−3.70	0.155
200	1.663	1.899	40, 334	−2.25	0.619	79, 337	−3.70	0.159
300	1.517	1.817	49, 332	−2.15	0.595	82, 327	−3.75	0.160
400	1.330	1.714	58, 327	−2.15	0.582	84, 326	−3.75	0.160

scenario, physical considerations suggest that the mass load(s) would lie near the great circle that includes our inferred TPW path (Fig. 3), that is, a path that keeps the pole ~90° from Tharsis.

Given the challenge of identifying evidence of ancient internal loads that may no longer have an observable signature, we briefly review candidate surface loads for the large Tharsis-driven TPW scenario. The gravity signatures of most major impact basins—such as the Argyre basin (Fig. 3), which lies along the inferred great circle path—indicate that they are not significant mass anomalies[15,20], and are therefore unlikely to have influenced the location of Mars' rotation pole. In contrast, the Elysium volcanic province and the Utopia impact basin (Fig. 3) are characterized by significant gravity highs[15], the latter owing to infilling by a large volume of material[21], and both lie on or near the great circle path. It is also interesting to note that the centroids of the Arabia and Deuteronilus palaeobasins (Fig. 3), which we calculated by subtracting the modelled deformation from the present topography, lie very close to the great circle defined by our inferred TPW path. Thus, loading and unloading of these basins with water and sediment might also have influenced the pole's position along this path, although the magnitude of this effect would depend on the geometry of the load redistribution (see Supplementary Information).

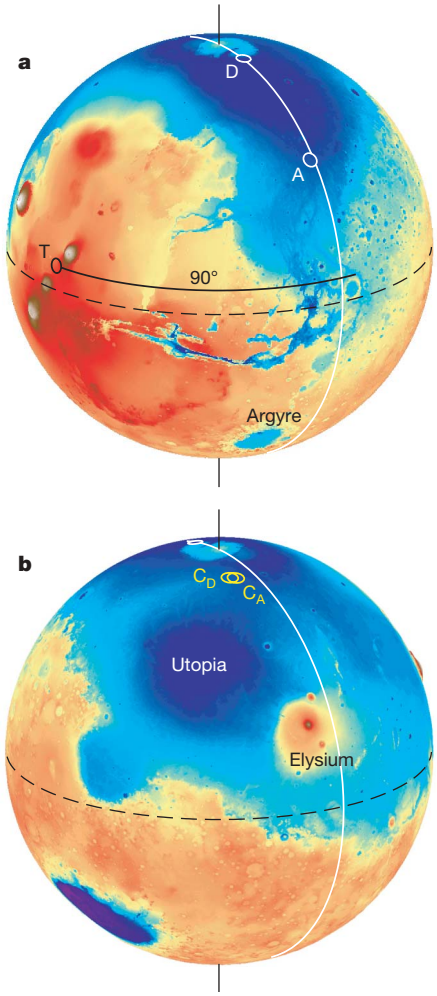

Figure 3 | TPW path that reconciles shoreline deformation. **a**, Best-fit palaeopoles inferred from the topography of the Arabia and Deuteronilus shorelines (small white circles labelled A and D) for $T_e = 200$ km (see Methods and Table 1), a value close to most recently published estimates for Mars' lithospheric thickness[25,28,29]. The palaeopoles fall along a great circle (white line) that follows the 335° E meridian. This great circle is nearly perpendicular to the Tharsis rise, as shown by the black line extending 90° east from the centre of Tharsis (black circle T). Palaeopoles for other values of T_e, which fall along the same great circle, are listed in the Methods. Orthographic spherical projection centred at 20° N, 30° E. **b**, View from the opposite side of Mars, showing the depth-weighted centroids of the Arabia (C_A) and Deuteronilus (C_D) palaeo-ocean basins. Orthographic spherical projection centred at 20° N, 210° E. Locations of the Argyre and Utopia impact basins and the Elysium volcanic rise are labelled. The present-day equator (dashed line) and rotation poles are shown in both panels.

Other processes may have contributed to the long-wavelength, large-amplitude topographic trends observed in the Arabia and Deuteronilus contacts. For example, the flexural response to the removal of the oceans would have altered the shoreline topography[22], but numerical calculations indicate that the amplitude of this response would be far too small to explain the observed trends or to affect the best-fit palaeopole locations significantly (see Supplementary Information). We also used similar numerical procedures to predict the flexural response to the development of the Tharsis rise. In this case, the amplitude can be significant[23], but the predicted trend, which diminishes with distance from Tharsis, does not match the elevation profile of either shoreline. Of course, this reasoning is also consistent with the conclusion that Tharsis was largely emplaced before the TPW episode we have invoked to explain the shoreline deformation.

The effect of internal loading on the observed shoreline deformation, either through the direct effect of dynamic topography[24,25] or via TPW-driven deformation, is difficult to assess. The greatest possible age difference between the Arabia shoreline, which may be as old as ~4 Gyr (ref. 7), and the Deuteronilus shoreline, which encircles the Hesperian age[10] Vastitas Borealis Formation and is therefore at least ~2 Gyr old, is ~2 Gyr, and the diminution with time of the observed long-wavelength trends is roughly a factor of four (Fig. 1). Thus, dynamic topography would have had to diminish in amplitude by a factor of four over a period of at most 2 Gyr, and subsequently a much smaller amount over a period of at least 2 Gyr. However, a transient convective event, such as wholesale overturn of the mantle due to thermochemical instability[26], might well attenuate in intensity on the timescale separating the Arabia and Deuteronilus shorelines, and thus contribute to the observed shoreline topography either directly through dynamic topography or indirectly by inducing TPW. As noted above, internal loading would be required to explain the inferred TPW path in Fig. 3 in the event that the growth of Tharsis drove relatively little TPW.

The long-wavelength deformation of the Arabia and Deuteronilus contacts has been used as a primary argument against their interpretation as shorelines, and has cast doubt on the idea that large standing bodies of water once existed on Mars. Our results support the hypothesis that the present topography of Mars, as sampled by the contacts, may not be representative of the topography at the time these features were formed. In particular, the difference is consistent with a TPW path that matches the expected rotational dynamics of Mars. The plausibility of an ancient northern ocean suggests several possible features that should serve as a focus for current and future Mars exploration, including the preservation of coastal and submarine sedimentary features such as transgressive–regressive sequences and turbidites, and the presence of relict ice in the sediments of the northern lowlands.

METHODS

We use fluid Love number theory to calculate the topographic response to a TPW event. Consider the initial rotational state shown in Fig. 2a, where (θ', ψ') are the colatitude and east longitude of the ancient north rotation pole. The centrifugal potential in this configuration at an arbitrary observation site (θ, ψ) is given by[27]:

$$\phi(\theta,\psi) = \frac{1}{3}\omega^2 a^2 - \frac{1}{3}\omega^2 a^2 P_{2,0}(\cos\gamma) \quad (1)$$

where ω and a are the rotation rate and mean radius, and γ is the angular distance between the observation site and the rotation pole (Fig. 2a). The function $P_{2,0}$ is the unnormalized degree-two, order-zero Legendre polynomial: $P_{2,0}(\cos\eta) = \frac{1}{2}(3\cos^2\eta - 1)$.

Assuming no change in ω, the perturbation in the centrifugal potential at (θ, ψ) as the rotation vector wanders from the initial orientation to the present one (Fig. 2b) is:

$$\Lambda(\theta,\psi) = \frac{1}{3}\omega^2 a^2 [P_{2,0}(\cos\gamma) - P_{2,0}(\cos\theta)] \quad (2)$$

Equation (2), represented graphically in Fig. 2c, describes the geometry of the topographic response to TPW. The amplitude of the response is[12]:

$$\Delta T(\theta,\psi) = \frac{\Lambda(\theta,\psi)}{g}\left[h_f - (1+k_f)\right] + Z \quad (3)$$

where g is the surface gravitational acceleration, the parameters h_f and k_f are the degree-two fluid h and k tidal Love numbers, and Z is a constant included because the sea surface potential at the time of shoreline formation is not necessarily the same as the potential that defines the present geoid. The fluid Love numbers are functions of Mars' density structure[28] and lithospheric thickness. Table 1 lists calculated values of h_f, which governs the solid surface displacement, and $(1 + k_f)$, which governs the geoid or sea surface displacement, as a function of the elastic thickness of the lithosphere T_e.

For each shoreline, we identified the palaeopole location and the value of Z that minimize the root-mean-square deviation ($\sigma_{r.m.s.}$) between equation (3) and the unsmoothed shoreline topography in Fig. 1. Best-fit palaeopoles and $\sigma_{r.m.s.}$ values for $100\,\text{km} \le T_e \le 400\,\text{km}$ (a range that encompasses most estimates for Mars[25,28,29]) are listed in Table 1.

Received 23 November 2006; accepted 18 April 2007.

1. Parker, T. J., Saunders, R. S. & Schneeberger, D. M. Transitional morphology in west Deuteronilus Mensae, Mars: Implications for modification of the lowland/upland boundary. *Icarus* **82,** 111–145 (1989).
2. Baker, V. R., Strom, R. G., Gulick, V. C., Kargel, J. S. & Komatsu, G. Ancient oceans, ice sheets and the hydrological cycle on Mars. *Nature* **352,** 589–594 (1991).
3. Parker, T. J., Gorsline, D. S., Saunders, R. S., Pieri, D. C. & Schneeberger, D. M. Coastal geomorphology of the Martian northern plains. *J. Geophys. Res.* **98,** 11061–11078 (1993).
4. Head, J. W. *et al.* Oceans in the past history of Mars: Tests for their presence using Mars Orbiter Laser Altimeter (MOLA) data. *Geophys. Res. Lett.* **25,** 4401–4404 (1998).
5. Head, J. W. *et al.* Possible ancient oceans on Mars: evidence from Mars Orbiter Laser Altimeter data. *Science* **286,** 2134–2137 (1999).
6. Ivanov, M. A. & Head, J. W. Chryse Planitia, Mars: Topographic configuration, outflow channel continuity and sequence, and tests for hypothesized ancient bodies of water using Mars Orbiter Laser Altimeter (MOLA) data. *J. Geophys. Res.* **106,** 3275–3296 (2001).
7. Clifford, S. M. & Parker, T. J. The evolution of the martian hydrosphere: implications for the fate of a primordial ocean and the current state of the northern plains. *Icarus* **154,** 40–79 (2001).
8. Carr, M. H. & Head, J. W. Oceans on Mars: An assessment of the observational evidence and possible fate. *J. Geophys. Res.* **108,** 5042, doi:10.1029/2002JE001963 (2003).
9. Malin, M. C. & Edgett, K. S. Oceans or seas in the Martian northern lowlands: High resolution imaging tests of proposed coastlines. *Geophys. Res. Lett.* **26,** 3049–3052 (1999).
10. Tanaka, K. L. & Scott, D. H. Geologic map of the polar regions of Mars. *US Geol. Surv. Misc. Invest.* Map I-1802C (1987).
11. Sabadini, R., Doglioni, C. & Yuen, D. A. Eustatic sea level fluctuations induced by polar wander. *Nature* **345,** 708–710 (1990).
12. Mound, J. E. & Mitrovica, J. X. True polar wander as a mechanism for second-order sea-level variations. *Science* **279,** 534–537 (1998).
13. Gold, T. Instability of the Earth's axis of rotation. *Nature* **175,** 526–529 (1955).
14. Willemann, R. J. Reorientation of planets with elastic lithospheres. *Icarus* **60,** 701–709 (1984).
15. Smith, D. E. *et al.* The gravity field of Mars: results from Mars Global Surveyor. *Science* **286,** 94–97 (1999).
16. Zuber, M. T. & Smith, D. E. Mars without Tharsis. *J. Geophys. Res.* **102,** 28673–28686 (1997).
17. Matsuyama, I., Mitrovica, J. X., Manga, M., Perron, J. T. & Richards, M. A. Rotational stability of dynamic planets with elastic lithospheres. *J. Geophys. Res.* **111,** E02003, doi:10.1029/2005JE002447 (2006).
18. Arkani-Hamed, J. & Boutin, D. Paleomagnetic poles of Mars: revisited. *J. Geophys. Res.* **109,** E03011, doi:10.1029/2003JE002229 (2004).
19. Hood, L. L., Young, C. N., Richmond, N. C. & Harrison, K. P. Modeling of major martian magnetic anomalies: Further evidence for polar reorientations during the Noachian. *Icarus* **177,** 144–173 (2005).
20. Zuber, M. T. *et al.* Internal structure and early thermal evolution of Mars from Mars Global Surveyor topography and gravity. *Science* **287,** 1788–1793 (2000).
21. Searls, M. L., Banerdt, W. B. & Phillips, R. J. Utopia and Hellas basins, Mars: Twins separated at birth. *J. Geophys. Res.* **111,** E08005, doi:10.1029/2005JE002666 (2006).
22. Leverington, D. W. & Ghent, R. R. Differential subsidence and rebound in response to changes in water loading on Mars: Possible effects on the geometry of ancient shorelines. *J. Geophys. Res.* **109,** E01005, doi:10.1029/2003JE002141 (2004).
23. Willemann, R. J. & Turcotte, D. L. The role of lithospheric stress in the support of the Tharsis rise. *J. Geophys. Res.* **87,** 9793–9801 (1982).
24. Redmond, H. L. & King, S. D. A numerical study of a mantle plume beneath the Tharsis Rise: Reconciling dynamic uplift and lithospheric support models. *J. Geophys. Res.* **109,** E09008, doi:10.1029/2003JE002228 (2004).
25. Roberts, J. H. & Zhong, S. Plume-induced topography and geoid anomalies and their implications for the Tharsis rise on Mars. *J. Geophys. Res.* **109,** E03009, doi:10.1029/2003JE002226 (2004).
26. Elkins-Tanton, L. T., Zaranek, S. E., Parmentier, E. M. & Hess, P. C. Early magnetic field and magmatic activity on Mars from magma ocean cumulate overturn. *Earth Planet. Sci. Lett.* **236,** 1–12 (2005).
27. Lambeck, K. *The Earth's Variable Rotation* (Cambridge Univ. Press, Cambridge, UK, 2005).
28. Sohl, F. & Spohn, T. The interior structure of Mars: Implications from SNC meteorites. *J. Geophys. Res.* **102,** 1613–1636 (1997).
29. Banerdt, W. B., Golombek, M. P. & Tanaka, K. L. in *Mars* (eds Kieffer, H. H., Jakosky, B. M., Snyder, C. W. & Matthews, M. S.) 249–297 (Univ. Arizona Press, Tucson, Arizona, 1992).
30. Webb, V. E. Putative shorelines in northern Arabia Terra, Mars. *J. Geophys. Res.* **109,** E09010 (2004).

Supplementary Information is linked to the online version of the paper at www.nature.com/nature.

Acknowledgements This work was supported by the NASA Astrobiology Institute (J.T.P. and M.M.), a Reginald A. Daly Postdoctoral Fellowship (J.T.P.), the Miller Institute for Basic Research in Science (J.X.M.), and NSERC (J.X.M.).

Author Contributions All authors contributed equally to this work.

Author Information Reprints and permissions information is available at www.nature.com/reprints. The authors declare no competing financial interests. Correspondence and requests for materials should be addressed to J.T.P. (perron@eps.harvard.edu).

doi: 10.1038/nature05873

Supplementary Information to accompany "Evidence for an ancient Martian ocean in the topography of deformed shorelines"

J. Taylor Perron[1], Jerry X. Mitrovica[2], Michael Manga[1], Isamu Matsuyama[3] & Mark A. Richards[1]

[1]*Department of Earth & Planetary Science, University of California, Berkeley, CA, USA*

[2]*Department of Physics, University of Toronto, Ontario, Canada*

[3]*Department of Terrestrial Magnetism, Carnegie Institution of Washington, Washington, DC, USA*

The long-term reorientation of the Martian rotation pole is governed by non-hydrostatic, or more accurately non-equilibrium, contributions to the inertia tensor or, equivalently, the degree two geoid[14,17]. These contributions will include any surface mass loads that are not perfectly compensated, internal (convective) heterogeneities, and the so-called remnant rotational bulge[14,17]. The latter refers to the portion of the rotational bulge which, due to the development of an elastic lithosphere, will not relax completely, even at infinite time, in response to a change in the rotation vector.

TPW driven by Tharsis

Following Willemann[14], the size of an axisymmetric surface load is conveniently expressed in terms of a parameter Q', defined as the ratio of the degree two, order zero component of the load (when the axis of the coordinate system is placed at the centre of the load), assuming no isostatic compensation, to the size of the (total) rotational bulge. For a load q, with units of stress,

Willemann[14] (Eqs. 17–18) expresses this ratio as

$$Q' = \left(\frac{C-A}{MR^2}\right)^{-1} \int_{\mu=\mu_0}^{1} \frac{q(\phi)}{\bar{\rho} g \bar{R}} \frac{3}{2} P_{2,0}(\mu) \mathrm{d}\mu \,, \tag{S1}$$

where ϕ is angular distance from the centre of the load, ϕ_0 is the angular distance to the edge of the load, $\mu = cos\phi$, $\bar{\rho}$ is the planetary mean density (3940 kg m^{-3}), $\bar{R}$ is the planetary mean radius (3397 km), $(C-A)/MR^2$ is the difference between the two principal moments of inertia before the emplacement of the load (0.0019), and $P_{2,0}$ is the degree two, order zero Legendre polynomial, as defined in the Methods Section.

The ability of a surface load of size Q' to drive TPW is dependent on a term $1 + k_f^L$, where k_f^L is the degree two fluid load Love number for the Mars model, which governs the level of load compensation ($1 + k_f^L$ approaches zero as the thickness of the elastic lithosphere is decreased). Moreover, the size of the remnant rotational bulge depends on a term $k_f^* - k_f$, where k_f is (as defined in the Methods Section) the degree two fluid tidal Love number (see Table 1 in the main text), while k_f^* is the value of k_f in the case where the Mars model has a lithosphere with no elastic strength (i.e., $T_e \rightarrow 0$ in Table 1). We use the methodology outlined by Matsuyama et al.[17] (see their Fig. 2) to compute TPW given a load of size Q' and fluid Love numbers computed, as in Table 1, for different values of T_e. For the interior model of Sohl and Spohn[28] and $T_e = 200$ km, $1 + k_f = 1.899$ (as in Table 1), $k_f^L = -0.764$ and $k_f^* = 1.190$.

Willemann[14] estimated an upper-bound value of $Q'_T = 1.74$ for the size of Tharsis. In this case, if we assume that the pre-Tharsis rotation axis was aligned with the axis of the remnant bulge that formed as the planet cooled and the lithosphere thickened, the solution to the equations

governing rotational stability of an axisymmetric load requires that the final colatitude of Tharsis was greater than $\sim$75° (see Fig. 2B in ref. 17). That is, regardless of the initial colatitude of Tharsis, the final colatitude would have placed it near the equator defined by the contemporaneous pole. In reference to Figure 3 in the main text, the paleopole after loading by Tharsis must therefore have been in a location very close to the great circle path inferred on the basis of shoreline deformation. This provides further, strong support for this inference of post-Tharsis TPW.

If we specify the pole location following Tharsis-driven TPW, then the stability equations also yield solutions for the TPW angle. For example, if the development of Tharsis moved the pole to the present-day pole position, and thus placed Tharsis at a final colatitude of 83.3° (ref. 16), then (for $Q'_T = 1.74$) there are two possible TPW angles[14,17]: 11° or 79° for $T_e = 200$ km (ref. 17). Very similar TPW values would be obtained if we took the pole location after loading by Tharsis to coincide with the paleopole inferred from the deformation of the Arabia shoreline (Figure 3 of the main text). These results are relatively insensitive to the choice of T_e (ref. 17).

The ability of surface mass loads to drive post-Tharsis TPW is a strong function of the level of TPW driven by the Tharsis loading. In particular, the large ($\sim$80°) solution for Tharsis-driven TPW cited above yields a much less stable rotation pole than the small TPW solution. There is a straightforward physical explanation for this result. If Tharsis drove TPW of $\sim$80°, it would have brought the remnant equatorial bulge into close alignment with the great circle that includes our paleopole locations (Table 1 and Figure 3 in the main text). In this case, a load lying near this great circle (i.e., Elysium, Utopia or the ocean locations, as defined by the centroids in Figure 3) would

have less difficulty perturbing the pole location since the TPW would proceed along the equator of the remnant rotational bulge. In contrast, if Tharsis drove TPW of $\sim$10°, then subsequent TPW along our inferred great circle path would meet significantly more resistance from the remnant bulge, and the driving load would therefore have to be much larger. This physics is well illustrated by the simple ocean loading scenario described next.

TPW driven by ocean loading and unloading

Let us consider the special case cited above in which the rotation pole prior to the formation of the oceans, and subsequent to the development of Tharsis, was near its present-day location. If the hypothesis that oceans once filled the northern lowlands is correct, these oceans would have represented a substantial mass of water, covering roughly one third of Mars' surface and reaching depths of several kilometers[7,8]. It is logical to assess the effect this water load may have had on Mars' rotational stability. The alignment of the ocean centroids with the TPW path inferred from the shorelines (Fig. 3 in the main text) indicates that the sense of TPW would have been correct, but it remains to evaluate the size of the loads and the amount of TPW they might have caused. In this section we investigate the following sequence of events: (1) The formation of the Arabia ocean caused an excursion of the rotation pole to the location in Fig. 3, and the Arabia shoreline formed with the pole at this location; (2) when the ocean water receded, the rotation pole moved to its present location, deforming the shorelines; (3) the Deuteronilus shoreline formed while the rotation pole was at an intermediate location, either when the Arabia ocean had partially disappeared, or during a subsequent ocean-forming episode with a smaller extent; (4) this younger

shoreline was deformed as the pole moved to its final position near the present location.

To calculate the long-term response of the pole to the combined effects of both Tharsis and the ocean load, we use the formulation for non-axisymmetric loads presented by Matsuyama et al.[17]. In this formulation, Tharsis and the ocean are treated as point loads with differing values of Q'. This approach assumes that T_e remains unchanged between the Tharsis-driven and ocean-driven reorientations.

To calculate Q' for the Arabia and Deuteronilus oceans, we consider an axisymmetric ocean with depth $h(\phi)$, such that $q(\phi) = \rho_w g h(\phi)$ in Equation S1. To obtain $h(\phi)$ for each shoreline, we determined the volumes of the paleo-ocean basins—7.66×10^7 km^3 for Arabia, 1.73×10^7 km^3 for Deuteronilus—and the mean angular radius ϕ_0 of each ocean about its centroid, and approximated the shape of the ocean basins as a cosine curve with central depth h_0:

$$h(\phi) = \begin{cases} \frac{1}{2}\alpha h_0 \left[\cos\left(\pi \frac{\phi}{\phi_0}\right) + 1\right] & \phi \leq \phi_0 \\ 0 & \phi > \phi_0 \end{cases} . \tag{S2}$$

Values used for Arabia (Deuteronilus) were $h_0 = 4.00$ km (1.40 km) and $\phi_0 = 80^\circ$ (65°). The factor α accounts for the additional accommodation space created by isostatic compensation of the ocean water. For Airy compensation,

$$\alpha = 1 + \frac{\rho_w}{\rho_m - \rho_w} C_n \, . \tag{S3}$$

C_n is the degree of isostatic compensation at spherical harmonic degree n ($0 \leq C_n \leq 1$, with $C_n = 1$ corresponding to a fully compensated load), which reflects the partial support of the

load by stresses in the lithosphere. From Equation 27 of Turcotte et al.[31], C_n is calculated to be approximately 0.75 for $T_e = 200\,\mathrm{km}$ and $2 \leq n \leq 6$ (a range of wavelengths that brackets those of the oceans). If $\rho_m = 3500\,\mathrm{kg\,m^{-3}}$, $\alpha = 1.3$.

From Equations S1–S3, the values of Q' associated with the emplacement of ocean water in the northern plains are 0.0403 (Arabia) and 0.0123 (Deuteronilus). But there are additional contributions to the total ocean load. Just as the emplacement of the ocean water in the northern plains causes a positive geoid anomaly, the removal of this water from elsewhere on the planet, if partially uncompensated, causes a negative anomaly. The magnitude of the resulting contribution to the total load depends on the geometry of the water source region and C_n. If the source region is exactly antipodal to the destination (i.e., a cap centred on the south polar region) and C_n is the same as above, the two anomalies offset one another, and the redistribution of water has no net effect on Mars' rotational stability ($Q' = 0$ for both shorelines). Similarly, an ocean that originates in the crust beneath the northern lowlands will also have $Q' = 0$. In the case of a uniform depth water source, the maximum ocean load size results from a source that forms an equatorial band extending from about -10° to 10° latitude. If $C_n = 0.75$ ($T_e = 200\,\mathrm{km}$), the Q' values associated with the water source are 0.0304 (Arabia) and 0.0072 (Deuteronilus). Adding these to the Q' values calculated above for the emplacement of water in the northern plains gives maximum possible ocean load sizes, Q'_O, of 0.0707 (Arabia) and 0.0195 (Deuteronilus).

In calculating these effective ocean load sizes, we make no assumptions about the processes that transported the water from its source region into the northern plains; we assume only that the

total mass of water was conserved. Deposition of lava or sediment could have increased the mean density of the load filling the northern plains, resulting in higher Q' values than those calculated here.

Figure S1 shows predictions of ocean-driven TPW as a function of Q'_O for the cases in which Tharsis drove a large (present latitude of pre-Tharsis pole $= 11°$) or small ($79°$) TPW event. These predictions, based on a simplified loading scenario, indicate that the Arabia and Deuteronilus oceans could have been sufficient to drive the TPW inferred from the long-wavelength deformation of the shorelines *only* in the case where Tharsis had driven an earlier, significant TPW event.

The ocean loading/unloading scenario described above is not unique, and the post-Tharsis polar motion required to fit the deformed shorelines (Table 1, Fig. 3) may also involve loading from other surface masses, including the Utopia impact basin or the Elysium volcanic province. Moreover, internal loads may also have played an important role in the rotational history of Mars; indeed, in the case of small Tharsis-driven TPW, the calculations in Fig. S1 indicate that such a contribution would be essential to reconcile our inferred (Fig. 3) pole path.

Regardless of the nature of the loading history, the combined contributions from rotational oblateness, remnant bulge reorientation and any uncompensated external and internal loads should yield a gravity field at spherical harmonic degree two that is consistent with observational constraints on the J_2 and $J_{2,2}$ harmonics of Mars. However, a direct comparison between the J_2 and $J_{2,2}$ signals from loading and TPW scenarios that reconcile the Arabia and Deuteronilus shoreline deformation with present-day observations may be somewhat misleading. In particular, internal

loading that post-dates these scenarios may contribute to the present-day gravitational field without leading to significant TPW. An example would be any recent, internally driven excess ellipticity of the planet—this signal would stabilize the pole, but not move it from its present position.

Nevertheless, in work to be reported elsewhere[32], we consider a number of Tharsis loading scenarios defined by varying Q' and T_e values and test their consistency with the present-day gravity field. The comparison assumes that the pre-Tharsis pole is aligned with the remnant rotational bulge, as in the analysis above, and that no other internal or external loads are active. It is straightforward to find acceptable small Tharsis-driven TPW scenarios within this procedure. In contrast, acceptable large Tharsis-driven scenarios are more difficult to find as a consequence of the large signal associated with any major readjustment of the remnant bulge. As an example, a scenario in which a Tharsis load with $Q' \sim 2.5$ produced a significant ($70°$) TPW event yields a misfit to the observed J_2 close to 7%, but much smaller misfits are found over a wide range of Q' values for the case in which Tharsis drove a smaller ($< 20°$) TPW event[32]. Thus, under the assumptions listed above, this analysis suggests that the present-day gravitational figure of Mars favours the small Tharsis-driven TPW scenario.

Flexural response of the shorelines to ocean unloading

In addition to creating extra accommodation space, the ocean load will induce flexural deformation of the lithosphere. For a perfectly axisymmetric ocean and a spatially uniform lithosphere, the flexural response will vary only with radial distance from the centre of the ocean, and the flexural

effect will not be apparent in topographic profiles along the circumference of the basin. As Leverington and Ghent[22] note, however, a non-axisymmetric ocean will induce a flexural response that varies along its margins. The subsequent deformation that occurs when such a load is removed will deform shorelines that formed while the ocean was in place. Given the non-axisymmetric shape of the Arabia and Deuteronilus basins (Figure 1 in the main text), this effect may be responsible for a component of the present-day shoreline topography.

To test the sensitivity of our inferred TPW paths to flexural effects, we removed the flexural signatures of the ocean loads from the present topography and determined the best-fit paleopoles for the corrected topography. The three-dimensional geometry of the ocean loads was determined by subtracting the TPW deformation (Equation 3 in the Methods section) from the present topography, flooding the paleotopography up to the mean elevation of the undeformed shorelines, and multiplying the resulting ocean depths by the compensation factor C_n (Equation S3) to account for the increase in ocean basin volume due to partial isostatic compensation of the water. We then calculated the flexural response to the removal of this spatially variable load at all locations where the shoreline elevations were sampled (Figure 1 in the main text). This calculation was performed using fluid h and k load Love numbers generated using the same suite of models listed in Table 1. In contrast to the rotational driving potential discussed in the Methods section (Figure 2 in the main text), the ocean mass load is comprised of a range of spatial scales; hence the flexural response was computed using load Love numbers up to spherical harmonic degree and order 256.

As an example, for $T_e = 200\,\mathrm{km}$, the maximum magnitude of the flexural response to the

ocean load is 177 m for the Arabia ocean and 113 m for Deuteronilus (Figure S2). We subtracted this flexural response from the present-day shoreline topography, and determined the best-fit paleopoles corresponding to the corrected shoreline elevations. The locations of the best-fit paleopoles are (42°N, 333°E) for Arabia, and (80°N, 332°E) for Deuteronilus, which differ by only a few degrees from the paleopoles determined by neglecting flexural effects (Table 1 in the main text). This indicates that neglecting the flexural effects of the ocean water in determining the paleopole location from the long-wavelength deformation of the Arabia and Deuteronilus shorelines is a very accurate approximation.

Additional References

31. Turcotte, D. L., Willemann, R. J., Haxby, W. F. & Norberry, J. Role of membrane stresses in the support of planetary topography. *J. Geophys. Res.* **86**, 3951–3959 (1981).

32. Daradich, A., Mitrovica, J. X., Matsuyama, I., Perron, J. T., Manga, M. & Richards, M. A. Rotational stability and figure of Mars. Submitted to *Icarus*.

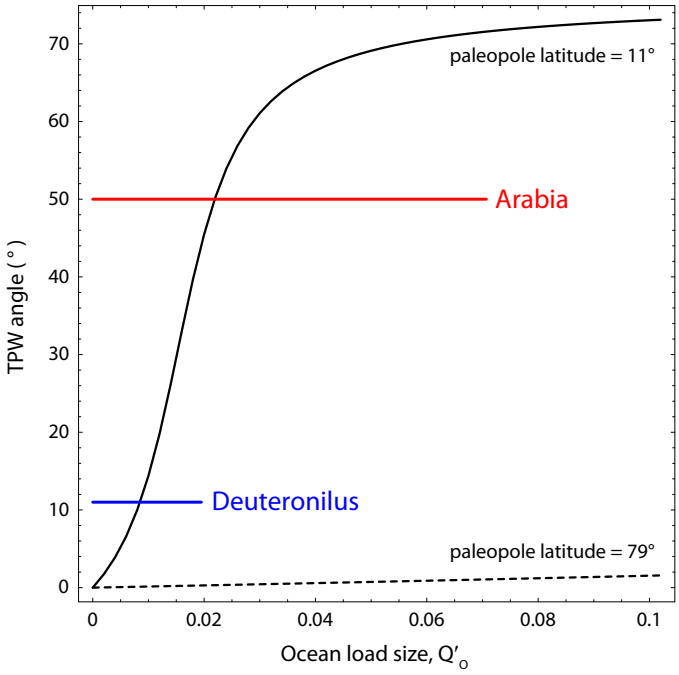

Figure S1: Magnitude of TPW, expressed as the angular distance between the initial and final rotation poles, caused by an ocean load of a given size for $T_e = 200$ km. Curves show numerical solutions calculated using the approach of Matsuyama et al.[17] for the two possible pre-Tharsis rotation poles described in the text: a pole closer to the present-day equator (solid), or one more closely aligned with the present pole (dotted). The widths of the horizontal bars show the range of possible sizes for each ocean load, and the vertical positions of the bars show the TPW angles required to generate the long-wavelength shoreline topography (Table 1 in the main text).

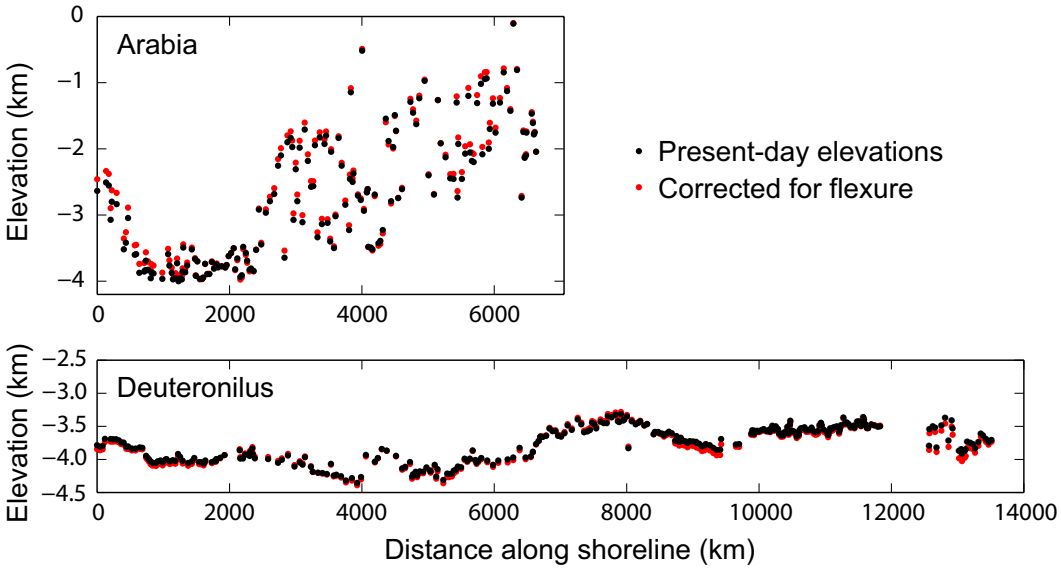

Figure S2: Change in the topography of the Arabia and Deuteronilus shorelines due to lithospheric flexure associated with the emplacement of a non-axisymmetric ocean load. Black points are present-day shoreline elevations from Carr and Head[8]. Red points are elevations following the emplacement of the ocean load for $T_e = 200\,\mathrm{km}$.